npj | computational materials

Article

Published in partnership with the Shanghai Institute of Ceramics of the Chinese Academy of Sciences

https://doi.org/10.1038/s41524-026-02130-w

Eigenmode following for direct entropy calculation and characterisation of magnetic systems

Check for updates

Stephan von Malottki[1,2,3,4] ✉, Moritz A. Goerzen[1,5], Hendrik Schrautzer[1,2], Pavel F. Bessarab[2,6] & Stefan Heinze[1,7] ✉

The effect of entropy can be crucial for magnetic skyrmions, and in some cases, its accurate prediction has been prevented by the limitations of the harmonic approximation. We present an eigenmode following method (EMF) that has been developed for the numerical scanning of the potential energy surface and the direct calculation of entropy and pre-exponential factors of transition rates. While the concepts of following eigenmodes and numerical direct entropy calculation have been known individually, their combination yields a new and general way of effective sampling of the energy surface for high-accuracy treatment of non-harmonic eigenmodes. For this, the EMF method requires iterative updates of the eigenpairs of the softest eigenmodes that need the most accurate modelling. In contrast to other methods, EMF does not move “uphill" or “downhill" in energy to find stationary points, but to obtain energy curves. By numerical integration of the Boltzmann factor along these curves, the partition functions of the following eigenmodes can be calculated without making assumptions of their form. We introduce the general theoretical background and algorithm of the EMF method before providing test calculations and relevant use cases in the framework of atomistic spin simulations with a focus on magnetic skyrmion collapse.

Various techniques to fully or partially explore potential energy surfaces (PES) have been developed in the past in order to study the stability and reactivity of solids, molecules and systems with multiple degrees of freedom in general[1–4]. Some “walk" on the PES to find local minima and transition states[2–10], while others, for example, the nudged elastic band method (NEB), energetically relax a reaction path to the minimum energy path (MEP) between an initial and final state, providing information about reaction mechanisms connecting these states[11–13]. In combination with statistical methods such as transition state theory (TST)[14–17] and related methods[18], knowledge of these points on the PES allows for the calculation of energy barriers and transition rates, typically written in the form of an Arrhenius law:

$$\nu = \nu_0 \, e^{-\beta \Delta E}. \tag{1}$$

Here, the transition rate, ν, is given by the pre-exponential factor, ν_0, the inverse of the thermal energy, $\beta = 1/k_B T$, and the energy barrier between the two states, ΔE. The energy barrier is defined as the energy difference between the transition state and initial state and can be obtained, for example, via the climbing image-NEB method (CI-NEB)[19]. The pre-exponential factor, ν_0, on the other hand, contains the dynamic and entropic components of the transition rate and is often more difficult to estimate[20–22].

In magnetism, variants of NEB have been used to study spin flip events[23], domain wall switching[23] and vortex switching[24,25], often in the context of thermal stability of magnetic bits[26]. However, it was the discovery of magnetic skyrmions in 2009[27], small topological, whirl-like structures, that motivated more sophisticated theoretical investigations[28–31]. By applying the geodesic nudged elastic band method (GNEB)[32], a variant of NEB that takes the constraint length of magnetic moments into account, the radial[22,32–34], chimera[35,36] and escape mechanisms[37] of skyrmion decay have been found and enabled the calculation of their corresponding energy

[1]Institute of Theoretical Physics and Astrophysics, University of Kiel, Leibnizstrasse 15, Kiel, Germany. [2]Science Institute, University of Iceland, 107 Reykjavík, Iceland. [3]Thayer School of Engineering, Dartmouth College, 15 Thayer Dr, Hanover, NH, USA. [4]UCLouvain, Institute of Condensed Matter and Nanosciences (IMCN), Chemin des Étoiles 8, Louvain-la-Neuve, Belgium. [5]Université de Toulouse, CNRS, CEMES, 29 rue Jeanne Marvig, Toulouse, France. [6]Department of Physics and Electrical Engineering, Linnaeus University, Kalmar, Sweden. [7]Kiel Nano, Surface, and Interface Science (KiNSIS), University of Kiel, Kiel, Germany. ✉e-mail: stephan.vonmalottki@uclouvain.be; heinze@physik.uni-kiel.de

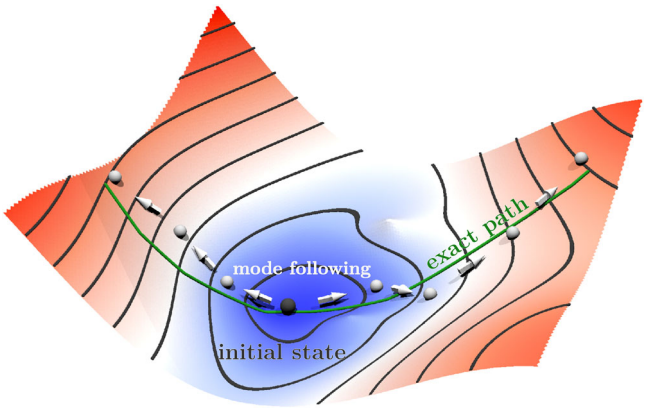


Fig. 1 | Illustration of the eigenmode following method. The shape and colour of the 2D function illustrate an arbitrary potential energy surface with a local energy minimum. From an initial state (black sphere), the eigenmode following method translates the system iteratively in small steps along the followed eigenvector, yielding an approximated path and energy curve of the eigenmode. The current eigenvectors (arrows) of the current state (white spheres) are recalculated each step.

barrier, ΔE. More recently, the first two mechanisms have also been identified experimentally[38]. Since the introduction of GNEB, the mechanisms and energy barriers of antiskyrmions[32,34,39,40], skyrmions in antiferromagnets[41], with higher-order exchange interactions[42], in multilayer systems[40,43,44], skyrmioniums[45], higher-order skyrmions[35], and skyrmions in 3D systems[46,47] have been investigated.

Further, the introduction of TST in harmonic approximation (HTST) to atomistic spin simulations[21,22,37,48] enabled the calculation of the pre-exponential factor and thus, mean lifetimes of skyrmionic textures in model systems[22,35,49,50] as well as realistic, DFT-parameterised ultrathin film systems[21,39,44,51]. The relevance of taking the prefactor into account was demonstrated experimentally in the chiral magnet $Fe_{1-x}Co_xSi$ by a dramatic change in prefactor by over 30 orders of magnitude over a small variation of magnetic field[52]. It was possible to calculate this entropic stabilisation effect for other materials via HTST as well and link it to the dependency of the prefactor on a few localised skyrmion eigenmodes[21,22,40,53].

We use the term eigenmode for a pattern of movement initially defined by the directions in the configuration space of magnetic textures, which correspond to eigenvectors of the Hessian matrix. However, the energy along some skyrmion eigenmodes cannot be modelled adequately in a harmonic approximation. Translation and rotational modes of skyrmions and antiskyrmions are often better treated in zero-mode, also called Goldstone mode[21,37], approximation, which assumes the energy to be constant along the eigenmode, while the rest of the spectrum is still treated in harmonic approximation[21,35,37]. Some magnetic states exhibit eigenmodes that do not fall into any of these two categories, limiting the applicability and accuracy of HTST to skyrmionics, especially for varying temperature regimes. For instance, the rotational modes of the Chimera saddle point structure, as well as the antiskyrmion ground state, prohibited the calculation of mean lifetimes in some studies[35,36]. The community was partially circumventing these issues by performing direct Langevin dynamics[54] or Monte Carlo[55] simulations, but these methods are limited by the rare event problem of skyrmions with high mean lifetime, which in turn can partially be mitigated by sophisticated but expensive forward-flux calculations[56].

While being powerful, the harmonic approximation has limitations that go beyond magnetism and skyrmionics alone and are well-known in other fields[57–60]. They can stem from the energy curves along eigenmodes not being shaped parabolically around the expansion point[20,57], the coupling of two or several eigenmodes[20,57] or a combination of both. There are ongoing efforts in many fields to find other feasible ways to calculate entropies without relying on the harmonic approximation, i.e., going "beyond harmonic" and it is an open question what approach is the most accurate and effective[20,61].

A common way to improve the description of the potential energy curve is to perform a fit with a better-suited formula. Examples are the free translator/rotor models[62], which are other names for the zero-mode approximation, a periodic potential, the so-called "hindered translator/rotator" models[63] or polynomials of third or fourth order[20,64,65]. However, it has been shown that these approximations can still fail in describing the energy along the curve adequately, leading to large errors in the calculated partition functions and consequently the entropies[20,58,59]. The promising "complete potential energy sampling" (CPES) method performs a direct numerical calculation of the entropy without relying on a pre-defined form of the energy curve and has been tested for diffusion processes[58]. The CPES method, however, requires explicit knowledge of several relevant points on the PES and a reasonable interpolation between them, which currently limits its generality[57,58]. Thus, a more general, robust method to calculate entropies "beyond harmonic" is needed.

In this work, we present the eigenmode following (EMF) method for accurately calculating anharmonic eigenmodes of the first kind, i.e. independently anharmonic modes with non-parabolic shaped energy curves for entropy and pre-factor calculations. Our approach combines the numerical evaluation of entropy by the sum over states formula[20] (Eq. (7), numerical) with eigenmode following and represents an effective way to sample the PES along the degrees of freedom that matter, i.e., along the soft eigenmode(s), while the unproblematic rest is calculated in harmonic approximation.

Note that in contrast to various well-established techniques[7,10,66,67], we do not use EMF to find stationary points on the PES but to classify individual eigenmodes and obtain their energy curves with numerical accuracy without approximating their form with any kind of formula. While methods proposed by Beste[20] as well as by Sauer and coworkers[64,65] perform small step EMF in linear response to fit higher-order polynomials to the obtained local energy curve, our EMF goes beyond this approach by iteratively updating the followed eigenvector as illustrated in Fig. 1. This allows accurate EMF over much larger distances, and thus, the direct numerical evaluation of the entropy for all occupied states along the eigenmode and not just strongly local information for fitting the parameters of a polynomial expansion.

For magnetic skyrmion collapse in ultrathin films such as Pd-fcc/Fe/Ir(111)[38,68], the effect of tunnelling is thought to be small[69]. Still, an adequate application of HTST for the calculation of mean skyrmion lifetimes has not been possible in several cases due to independent anharmonic eigenmodes. This limitation has motivated us to develop the EMF method in the first place, see ref. 53. We subsequently applied it to the skyrmion and antiskyrmion rotation modes in Rh/Co/Ir[39], the skyrmion collapse in multilayers of Pd-fcc/Fe/Ir(111)[43] and the chimera collapse transition[38,53]. More recently, we also successfully combined the EMF method with Monte Carlo simulations[70]. As the focus of this manuscript lies on the introduction of the method itself, we are limiting the presented use cases to the analysis of the chimera collapse mechanism.

In the following, the theoretical background and algorithm of EMF for direct entropy calculation are introduced in a general formulation that can be applied to different fields. Afterwards, test calculations and use cases are presented for magnetic systems described by the extended Heisenberg model with a focus on magnetic skyrmions. While we limit ourselves to the framework of quasi-classical atomistic spin simulations, we do believe that our EMF concept can be of use in other fields like diffusion, reaction kinetics or free energy stability calculations and combined with density functional theory or other quantum mechanical or classical computational frameworks.

Results

Eigenmode following for transition state theory

For the sake of clarity, we give a brief introduction to harmonic transition state theory here and refer to other publications with a more general and extensive explanation of the method[14–17,48,49,53]. At the very basic level, the main task in TST is to calculate the flux through the dividing surface, D,

which can be expressed by the following integral:

$$\nu = \int_{\mathrm{D}} \mathrm{e}^{-\beta E(\mathbf{Q})}\, \nu_{\perp}^{+}(\mathbf{Q})\, \mathrm{d}\mathbf{Q}. \tag{2}$$

Each state of the system is described by the generalised coordinates, $Q = q_1, \ldots, q_N$ and the component of the velocity perpendicular to D in the positive direction of the reaction is given by $\nu_{\perp}^{+}$

By applying the independent mode approximation[20], the pre-exponential factor of the Arrhenius law (see Eq. (1)) $\nu_0 = \nu/\Phi^{\mathrm{I}}$, the flux normalised to the partition function of the initial state, can be factorised to obtain the form

$$\nu_0 = \frac{\lambda}{\sqrt{2\pi\beta}} \frac{\prod_{n=2}^{3N} \Phi_n^{\mathrm{SP}}}{\prod_{n=1}^{3N} \Phi_n^{\mathrm{I}}}. \tag{3}$$

Here, λ contains the dynamic contribution of the transition (see ref. 49 for more details) and is computed via linearising the Landau-Lifshitz-Gilbert equation in harmonic approximation, as it is the standard procedure in TST. It depends exclusively on the precessional terms of the Landau-Lifshitz-Gilbert equation and is therefore independent of the material's damping factor. The ratio of products consists of the partition functions of the eigenmodes of the initial and saddle point (SP) states, Φ_n^{I} and Φ_n^{SP}, respectively. The number of atoms is given by N. The indices of the eigenmodes are ordered with increasing eigenvalues of the respective Hessian matrix. Note that the partition function of the first eigenmode of the SP, also referred to as the unstable mode, is excluded from the product, since states along this mode do not lie within the dividing surface.

Due to the decoupling of the eigenmodes, i.e., the independent mode approximation, their partition functions can be calculated individually via the line integral

$$\Phi_n = \int_{-\infty}^{\infty} e^{-\frac{\beta}{2}[E(q_n)-E_0]}\, \mathrm{d}q_n, \tag{4}$$

where q_n denotes the value of the eigenvector $\mathbf{q}_n$, whose orientation can change during the mode following process. $E(q_n)$ is the energy curve along q_n, and E_0 is the energy of the state at $q_n = 0$. The most common approximations of the energies $E(q_n)$ follow a Taylor expansion[20]:

$$E(q_n) \approx \underbrace{x_0}_{\text{zero mode}} + \underbrace{x_1 q_n}_{=0} + \underbrace{x_2 q_n^2}_{\text{harmonic}} \underbrace{+ x_3 q_n^3 + x_4 q_n^4}_{\text{higher order corrections}}. \tag{5}$$

Consequently, the approximations are named after the highest expansion parameter $x \neq 0$. Stationary points are defined by their first derivative equalling zero, and, thus, the first-order element vanishes.

In this work, we compare the partition functions obtained via three methods: Zero mode approximation, harmonic approximation and our EMF for direct calculation of the entropy, which is directly related to the partition functions Φ_n by

$$S = k_{\mathrm{B}} \left(\frac{N_h}{2} + \sum_{n=1}^{3N} \ln \Phi_n \right) \tag{6}$$

where N_h is the number of harmonic degrees of freedom. The corresponding formula for the partition function of the n-th eigenmode of the diagonalised Hessian matrix read:

$$\Phi_n = \begin{cases} V_n, & \text{zero mode}, \\ \sqrt{2\pi(\beta\epsilon_n)^{-1}}, & \text{harmonic}, \\ \sum_{k=1}^{K} \mathrm{e}^{-\beta\left[E\left(q_n^k\right)-E_0\right]} \Delta q_n^k, & \text{EMF}. \end{cases} \tag{7}$$

The zero mode volume, V_n, is independent of energies and the occupation of states. It equals the uniform integral over q_n and requires prior knowledge about it's symmetry. The partition function of the harmonic approximation depends on the thermal energy, β, and the eigenvalue of the n-th eigenmode, ϵ_n, which represents the curvature of the PES at the expansion point, i.e., the investigated state.

In the EMF calculation of entropy, the integral of Eq. (4) is replaced by a finite sum of small steps, k, along the eigencoordinate q_n with a step width of Δq_n^k. As illustrated in Fig. 1, these steps are performed iteratively along the n-th eigenmode. For each step, the energy is evaluated and used to calculate the Boltzmann factor, which yields the local contribution to the partition function when multiplied by the step width. In contrast to other methods, such as refs. 20,64,65, the EMF for direct entropy calculation does not require any explicit approximation of the PES and describes the energy curve with numerical precision as long as the mode tracking (see next section) is successful. Note that the EMF, as well as the above-mentioned approaches, rely on the independent mode approximation and, thus, a reasonable amount of orthogonality of the eigenvectors along the integrated path.

While each Φ_n can be calculated using a different approximation, it is the softest eigenmodes of a system that can have a strong effect on the overall transition rates. While showing only a small absolute error when modelled inadequately, their relative error can be dramatic due to the multiplication by the rest of the distribution function. It is a practical strategy to calculate the vast majority of Φ_n in harmonic approximation and use the more costly and accurate EMF for a few eigenmodes with the lowest eigenvalues.

Algorithm

Starting from a selected system configuration, Q_0, on the PES, typically the initial or SP state, the EMF method iteratively displaces the system configurations, Q_i, in the direction of the selected eigenvectors, ν_i^F, of the corresponding Hessian matrices. The following eigenvector is updated at each step to allow for long-range displacement, minimising distortions along the path. The algorithm, sketched in Fig. 2, consists of four primary steps:

1. Calculation of the eigenvalues, $\{\lambda_i^m\}$, and eigenvectors, $\{\nu_i^m\}$, of the system configuration Q_i.
2. Identify which eigenvector of $\{\nu_i^m\}$ is the most similar to ν_{i-1}^F (Mode tracking).
3. Displacement of the current configuration, Q_i, along the selected eigenvector ν_i^F.
4. Evaluation of the energy of the new state Q_{i+1}.

Here, m denotes the index of the eigenvalue in the ordered spectrum. In principle, the eigenpair spectra, $\{\lambda_i^m\}$ and $\{\nu_i^m\}$, can be obtained by direct diagonalisation of the Hessian matrix of the state Q_i. It consists of the second derivatives of the Hamiltonian with regard to the generalised coordinates, q_i. While this approach is straightforward, it is also often the computational bottleneck in large systems. In most cases, it is only necessary to treat eigenmodes at the lower end of the spectrum with EMF, as they are the softest and most likely eigenmodes to exhibit non-parabolic energy curves. Therefore, just the lowest few eigenpairs need to be calculated, and extremal eigensolvers can be utilised to significantly reduce the computational costs of the diagonalisation.

In order to further reduce the computational cost, other, more case-dependent optimisations can be applied. For example, a Hamiltonian without long-range interactions can result in a sparse Hessian matrix, which is the case for our extended Heisenberg model (see Eq. (9)) that we apply in the next sections. This allows us to use a state-of-the-art extremal sparse eigensolver[71] implemented in the Intel MKL library. The Hessian matrix can also be approximated as, for example, by finite difference approximations using the first order information of the gradients[9,72,73]. This flexibility of the method allows the user to find a physically and computationally sound implementation that suits the studied system the most to make it as fast and accurate as possible.

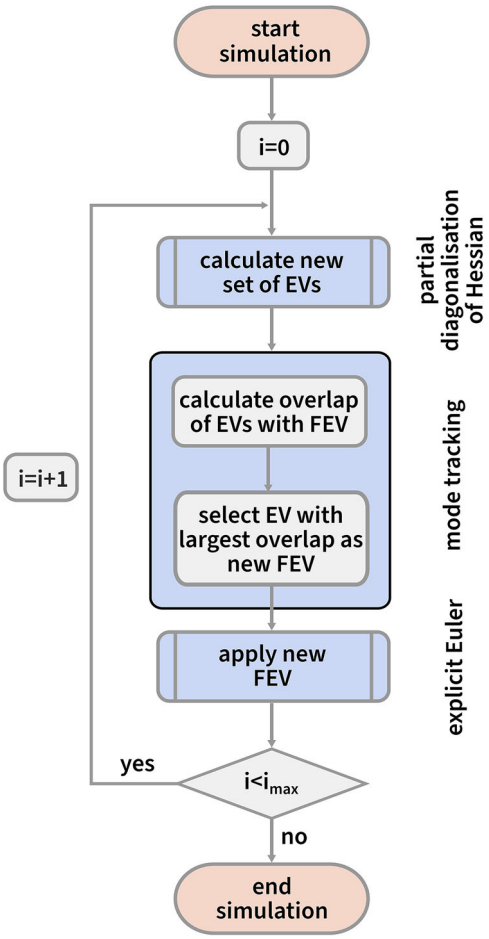


Fig. 2 | Abstract flow chart of the eigenmode following method. In the iterative loop, the three main subroutines are executed one after another: The partial or full diagonalisation of the Hessian, which yields a new set of eigenvalues and eigenvectors (EVs) for the current state. Then the mode tracking, which calculates the overlap of the previously followed eigenvector (FEV), v_i^F, with the new set of EVs and than select the one with the largest overlap as the next followed eigenvector, v_{i+1}^F. Finally, the newly found v_{i+1}^F is applied to the current state, Q_i, creating the next state, Q_{i+1}, as a basis for the next iteration cycle. The iteration stops when the maximum number of steps, a maximum distance of displacement or a certain energy is reached.

When the new eigenvectors, $\{v_i^m\}$, have been obtained, the next task is to identify which of them corresponds to the selected eigenmode to follow. In our EMF method, this means the "mode tracking" algorithm has to determine which new eigenvector is the most similar to the followed eigenvector of the previous iteration, v_{i-1}^F. In the first iteration, $i = 1$, the following eigenvector, v_1^F, is selected by the user. In the subsequent iterations, the overlap of the new eigenvectors with the previous v_{i-1}^F is calculated. In the framework of atomistic spin simulations, the eigenvectors are $2N$-dimensional vector fields in tangent space, and the overlap translates to simple scalar products of v_i^m and v_i^F.

In large systems, it is impractical to calculate the overlap of v_i^F with each individual eigenvector of the spectrum. Instead, we use the indexation of the eigenvectors in increasing eigenvalue order and the condition that the PES is continuously derivable twice. This means that a sufficiently small step on the PES results in a small change in the eigenspectrum, and thus, only a limited shift of the eigenvector indexation. This allows us to consider only a small interval of eigenvector indices around the index of v_{i-1}^F and to still ensure that we find the new eigenvector with maximum overlap. This procedure is illustrated in Fig. 3.

Note that mode tracking only works reliably when there are no hybridisations of eigenmodes in the considered interval of eigenvectors. If that is the case, the characters of the corresponding eigenmodes are changing, and the concept of following an eigenmode breaks down. An example would be the compression of a magnetic skyrmion until it is too small to be compressed further, and the corresponding eigenvector gets pushed far up the spectrum or even disappears entirely. Fortunately, this phenomenon is negligible for the numerical integration of the entropy (Eq. (7)) when the energy is increasing quickly enough while following the eigenmode for the Boltzmann factor to decay before the breaking point of mode following is reached.

After the new followed eigenvector, v_i^F, has been identified via mode tracking, it is applied to displace the current system configuration:

$$Q_i = Q_i + \Delta s\, v_i^F. \tag{8}$$

Here, Δs is the step width. The displacement can be performed with different numerical recipes, such as, for example, with an explicit Runge-Kutta algorithm or the Velocity Projection Optimisation (VPO) method[32]. The choice might depend on the studied system and the computational framework. Here, we apply a simple direct Euler integration scheme, which yields sufficient numerical stability and accuracy for the systems studied in this work. Note that for atomistic spin simulations, the configuration space is a $2N$-dimensional hypersphere and displacements have to be performed as rotations in the tangent space as described, for example, in refs. 32,53.

EMF in atomistic spin simulations

We have developed and tested the EMF method in the context of atomistic spin simulations, which apply a quasi-classical atomistic approximation to describe the magnetic moment of solid states. For all test and use cases presented in this work, the interactions of the magnetic moments are given by the extended Heisenberg model:

$$\begin{aligned} E \;=\; & -\sum_{i,j}^{N} J_{ij}(\mathbf{m}_i \cdot \mathbf{m}_j) - \sum_{i,j}^{N} D_{ij}(\hat{\mathbf{z}} \times \mathbf{r}_{ij}) \cdot (\mathbf{m}_i \times \mathbf{m}_j) \\ & - \sum_{i}^{N} K(\mathbf{m}_i \cdot \hat{\mathbf{z}})^2 - \sum_{i}^{N} \mu_i(\mathbf{m}_i \cdot \mathbf{B}) \,. \end{aligned} \tag{9}$$

It takes into account two-site exchange interactions beyond nearest neighbours, Dzyaloshinskii-Moriya interaction (DMI), magnetocrystalline anisotropy energy (MAE) and Zeeman interaction. Due to the constrained length of the magnetic moments, the configuration space changes from the general $3N$ to a $2N$-dimensional hypersphere with N being the number of atoms or magnetic moments, respectively.

The limitation of this specific model and field of application is not intrinsic to the EMF method but reflects our own scientific focus and expertise. However, it does allow for a quasi-classical treatment of the state space and an explicit construction of a Hessian matrix, which, due to the lack of dipole-dipole interaction, is sufficiently sparse for efficient sparse extremal eigensolver algorithms. In the following, two test cases of EMF are presented in order to illustrate and test the implementation. It is followed by the application of the EMF method to the chimera saddle point rotation mode, demonstrating a practical use-case in which transition rate calculations have not been possible otherwise.

Single spin: comparison of partial partition functions

Here, we consider a single magnetic moment in two configurations: Parallel and perpendicular to the uniaxial anisotropy axis $\hat{\mathbf{n}}$. We chose the calculation of the partial partition functions of this simple single-spin system because it already highlights and explains the limitations of the harmonic and zero-mode approximations and the capabilities of the EMF method. Simultaneously, it represents a suitable minimal first test case for a fresh implementation of the method.

The diagonalisation of the 2×2 dimensional Hessian matrix in tangent space coordinates results in two eigenmodes. For a magnetic moment in the easy axis direction, the two eigenmodes of the system are degenerate and

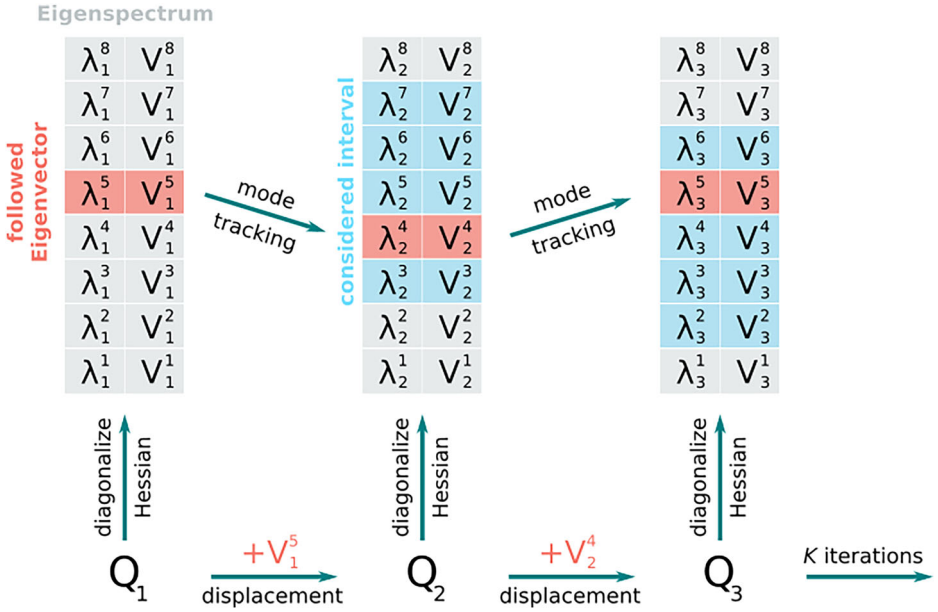


Fig. 3 | Illustration of the Mode tracking and the considered interval of the eigenspectrum. An initial state Q_1 is diagonalised, yielding the ordered eigenspectrum with eigenvalues, $\{\lambda_1^m\}$, and their corresponding eigenvectors, $\{v_1^m\}$. In this example, we assume that the fifth eigenmode should be followed, so Q_1 is displaced in the direction of v_1^5, creating the next state in the iteration, Q_2. This time, a certain interval centred around the previously selected eigenvector, here v_1^5, is chosen, here with two eigenpairs above and below index 5. In the second iteration, the eigenvector V_2^4 has maximum overlap with V_1^5 and is applied to Q_2 in order to calculate Q_3. This procedure is repeated for K iterations.

correspond to a rotation from one pole over the equator towards the other pole, as illustrated in Fig. 4(a, b). When assuming the magnetic moment to be oriented in the hard plane, which coincides with the saddle point of a pole-to-pole transition, the diagonalisation yields the two eigenmodes shown in Fig. 4(c, d). The first one is of the same nature as the two degenerate eigenmodes of the energy minimum, but with a phase shift of $\pi/2$. The second eigenmode describes a movement around the equator with constant energy of $E = K$.

The partial partition functions, Φ_p, introduced in Eq. (4), equal the statistical occupation of states along the eigenmodes with index $p = 1, 2$. In this example, we assume a temperature of $T = 10$ K and a MAE constant of $K = 1$ meV. The corresponding eigenvalues of the degenerate eigenmodes of the moment along $\hat{\mathbf{n}}$ are $\lambda_{1,2}^{\parallel} = 2$ meV, and the two eigenvalues of the moment perpendicular to $\hat{\mathbf{n}}$ are $\lambda_1^{\perp} = 2$ meV and $\lambda_2^{\perp} = 0$ meV. Table 1 shows the values of the partial partition functions in Eq. (4) determined via different techniques. The values of Φ_p are calculated for a full rotation over ϑ and φ, respectively, and details on the calculations are given in the "Methods" section. The method coined "ref" serves as a reference and corresponds to the simple numerical integration of the Φ_p integrals, made possible by the straightforward geometry of this test case.

The two degenerate eigenmodes of $\mathbf{m} \parallel \hat{\mathbf{n}}$ show the same behaviour: The harmonic approximation reproduces some parts of the actual energy curve (which has been obtained by EMF) well, but does not capture the periodic behaviour (see Fig. 4(a, b)). That shortcoming can be mitigated by adding a second parabola around $q_1 = \pi$, which results in a factor of two in the integration over a full period (see methods) and a value of Φ_p which is close to the reference. However, the slightly lower values stem from the harmonic approximation underestimating the occupation around the peaks of the oscillation. The EMF method, in contrast, does take the real energy curve into account and agrees with the reference perfectly. The zero-mode approximation, on the other hand, overestimates the occupation as each state has an energy cost of zero, yielding a value of $\Phi_p = 2\pi$.

In the case of the first eigenmode of $\mathbf{m} \perp \hat{\mathbf{n}}$, the energy curve is effectively shifted by an angle of $\pi/2$, which the EMF method can correctly capture, reproducing the value of the reference. The harmonic approximation, on the other hand, cannot be applied via Eq. (7), as the curvature and eigenvalue are negative, and the square root does not result in a real number. The zero mode approximation expanded around the initial state of $\mathbf{m} \perp \hat{\mathbf{n}}$ overestimates the energy drastically and thus underestimates the occupation, which shows in the much lower value of Φ_p in Table 1. This is different for the second eigenmode of $\mathbf{m} \perp \hat{\mathbf{n}}$, in which the zero mode approximation perfectly describes the energy along the rotation, agreeing with the Φ_p values of both the EMF method and the reference. Again, the harmonic approximation does not lead to a Φ_p value, as it would mean a division by zero in Eq. (7).

In summary, this simple example showed that the harmonic approximation tends to underestimate occupations with elevated temperatures (relative to the internal energy barriers, in this case, the anisotropy). On the other hand, the zero-mode approximation did drastically overestimate the occupation for $\mathbf{m} \parallel \hat{\mathbf{n}}$ in which the internal barriers were not negligible, while overestimating it for the first eigenmode of $\mathbf{m} \perp \hat{\mathbf{n}}$ and working precisely for the second eigenmode. This demonstrates very clearly that the usefulness of these approximations is strongly case-dependent. In contrast, the EMF method produced correct values for all four cases and, on top of that, provided the actual energy curves along the eigenmodes, making the physical understanding of their respective characters and judgments about the validity of the harmonic and zero-mode approximations possible.

Ferromagnet: numerical limits of integration

Here, we are investigating the eigenmodes of the ferromagnetic state, i.e., spin waves in a 50 × 50 hexagonal simulation box of the Pd-fcc/Fe/Ir(111) system (material parameters in ref. 34). In Fig. 5, the energy curves of the lowest three eigenmodes obtained by EMF are displayed up to the limit of 50 meV/atom, which corresponds to an average temperature of 380 K. While linear spin waves can be expected to be well described in harmonic approximation, it was not known a priori if that is true in a system like Pd-fcc/Fe/Ir(111) with its strong exchange frustration. Hence, the dashed lines created from the eigenvalues of the Hessian matrix are compared to the energy curves of EMF and reveal that the exchange frustrated spin waves of this system can indeed be modelled in harmonic approximation. The two lines can hardly be distinguished from one another.

To test the cutoff parameter of the numerical integration, $q_p^{\max}$, the partition function, Φ_1, of the first spin wave mode has been calculated with different values of the maximal displacement (see Fig. 6). In that process, the mode has been followed in positive and negative direction of the eigenvector until $|q_1^{\max}|$ is reached in both directions and the contributions are added to yield Φ_1 as described in Eq. (7).

In Fig. 6, the values of Φ_1 evaluated with EMF are converging with increasing $|q_1^{\max}|$ against the corresponding dashed lines of the harmonic approximations. This convergence was expected, as we already demonstrated that the harmonic approximation is a valid description of this eigenmode. The partition functions of lower temperatures are converging

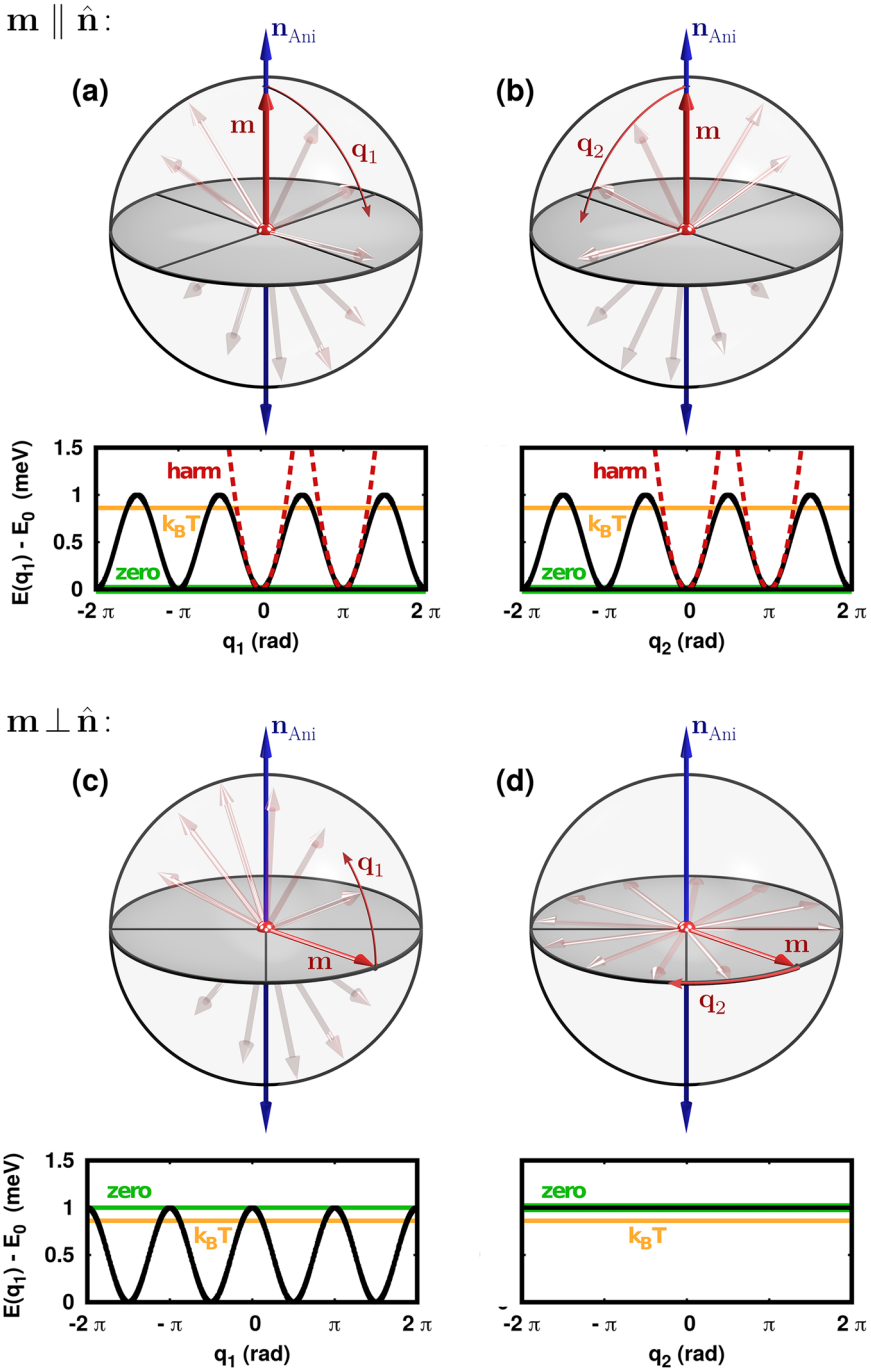


Fig. 4 | Illustration of the eigenmodes of a single spin system with uniaxial anisotropy. The magnetic moment, **m**, is assumed to be parallel (**a**, **b**) or perpendicular (**c**, **d**) to the easy axis of the anisotropy, $\hat{\mathbf{n}}_{\mathrm{Ani}}$. Each of these two states has two eigenmodes, illustrated by the transparent red arrows. The energy of each eigenmode is plotted for a full rotation in clockwise and anti-clockwise directions. The energy obtained by EMF along q_p is shown as a solid black line relative to the minimum energy, E_0. For this example, an anisotropy constant of K = 1 meV and a temperature of T = 10 K have been assumed, and the corresponding thermal energy is displayed as $k_B T$.

faster as their respective Boltzmann factors decline more quickly with increasing excitation energy, resulting in a smaller required distance to reach less occupied states. Overall, Fig. 6 demonstrates that the evaluation of partition functions with EMF converges as expected, fast enough and in a displacement interval that is realistically feasible.

EMF applications for magnetic skyrmion collapse

The dominating mechanism of magnetic skyrmion annihilation depends on the material parameters and external stimuli[35,36,38,53]. In case of a large DMI, a strong exchange frustration or effects that break the in-plane symmetry of the skyrmion, such as an in-plane magnetic field, skyrmions tend to decay via the so-called chimera collapse mechanism[38,53].

As an example, we are using the ultrathin film system Pd-fcc/Fe/Ir(111), a theoretically[34,50,53,55,74–76] as well as experimentally[38,68,77–79] well-studied model system with strong exchange frustration and DMI, in which sub-5 nm skyrmions occur at low temperatures below 80 K[79]. The minimum energy paths of a skyrmion collapsing in Pd-fcc/Fe/Ir(111) via the radial and chimera transition mechanisms are shown in Fig. 7. At the selected field of B_z = 4.0T, the energy barriers of both mechanisms are of comparable size, with the radial mechanism exhibiting a slightly lower barrier than the chimera one.

After its theoretical discovery[35,36], the calculation of the entropic contribution of the chimera collapse was prevented by the inability to handle the second eigenmode of the chimera saddle point state, the rotational eigenmode[36]. Only later, investigations via the EMF method[53] and subsequent analytical parametrization[39] have solved the puzzle on how to treat this eigenmode correctly.

In this section, we want to focus on the application of the EMF method to the rotation mode of the chimera transition state in Pd-fcc/Fe/Ir(111). In the first part, we introduce the challenge of treating the rotational eigenmode

in harmonic approximation and discuss the results obtained by EMF. In the second part, we increase the complexity of the energy surface by the consideration of an in-plane magnetic field, such as in the experimental setup of ref. 38, demonstrating the potential of the EMF method to accurately calculate entropies continuously even for intermediate temperature regimes.

Rotation of the chimera saddle point state

At its saddle point state, which is the state of maximal energy on the MEP (see Fig. 7), the second Hessian eigenmode exhibits a small eigenvalue of ≈ 0.1 meV, which lies between the typical order of magnitudes for zero eigenmodes (< 10^{-3} meV) and harmonic eigenmodes (> 1.0 meV) of that system. Thus, it was an open question for which temperatures the treatment in harmonic approximation would be valid. Alternatively, the modelling in zero-mode approximation came with the issue of not knowing the symmetry of that eigenmode, which we now know as the chimera rotation mode. Hence, the correct modelling of the chimera rotation mode remained an open question until we applied the EMF method to reveal its nature.

In Fig. 8, the magnetic structure of the chimera SP can be seen at "0.0" displacement. The corresponding second eigenvector of the Hessian matrix is displayed as a 2D vector field below. At first glance, it resembles known skyrmion translation mode eigenvectors[53]. By iteratively displacing the magnetic structure of the chimera saddle point state along this eigenvector and updating the latter along the way, i.e., "following" it, we obtain the snapshots of the magnetic structure and eigenvector displayed in Fig. 8. They reveal a rotational movement of the chimera saddle point around its Bloch-like point. The eigenvector follows the structure well and with good precision. In Fig. S1 of the supplemental figure, we performed a long-range mode following of several full rotations and highlighted the good numerical stability of the method.

By simultaneously evaluating the energy of the magnetic state along the movement, the corresponding energy curve over the displacement distance can be obtained as plotted on the left side of Fig. 8 for a 120° rotation, so one-third of a full rotation. The energy variation along the movement is relatively small and on the order of 0.1 meV. It is caused by the lattice effect that forces the Bloch-like point to slightly change its configuration during the rotation, leading to a 6-fold symmetry over a full rotation. The energy peaks are elevated and reduced by DMI, respectively, as the rotational sense in the

Table 1 | Values of Φ_p for a single spin with uniaxial anisotropy

Φ_p		Harmonic	Zero-mode	EMF	Ref
$\mathbf{m} \parallel \hat{\mathbf{n}}$	mode 1	3.291	6.283	3.819	3.819
	mode 2	3.291	6.283	3.819	3.819
$\mathbf{m} \perp \hat{\mathbf{n}}$	mode 1	-	1.969	3.819	3.819
	mode 2	-	1.969	1.969	1.969

The partial partition function, Φ_p, has been calculated for two initial magnetic moment orientations, $\mathbf{m} \parallel \hat{\mathbf{n}}$ and $\mathbf{m} \perp \hat{\mathbf{n}}$. The calculation methods are: harmonic approximation, zero-mode approximation and EMF, as shown in Eq. (7) and a reference obtained from directly solving the integral over the Boltzmann occupation numerically. The parameters are $K = 1$ meV and $T = 10$ K. More details of the calculations are given in the "Methods" section.

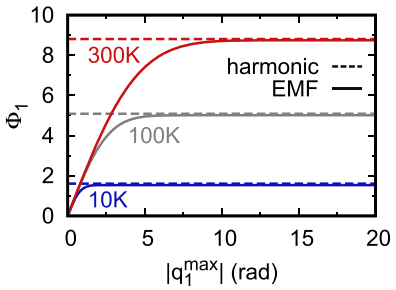


Fig. 6 | Value of Φ_1 of the first spin wave mode over the maximal EMF integration distance, q_1^{max}. The numerical integration of the Boltzmann factor has been performed for three different temperatures, and the corresponding integrals solved analytically via the harmonic approximation are shown as dashed lines. Figure adapted from ref. 53.

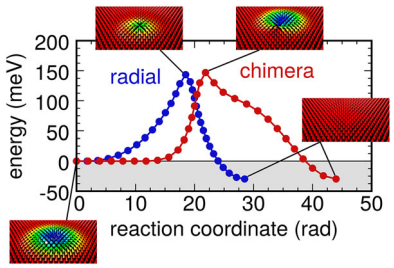


Fig. 7 | Minimum energy paths of skyrmion collapse via radial and chimera transition mechanisms. The same skyrmion obtained in Pd-fcc/Fe/Ir(111) at an external magnetic field of 4.0 T perpendicular to the surface exhibits two metastable transition mechanisms, the radial and the chimera collapse. The paths are obtained by CI-GNEB. The initial state is the skyrmion (zero on the reaction coordinate, spin structure shown as an inset), and the energy is given with respect to the skyrmion state. Each point corresponds to one intermediate state, so-called "images". For both mechanisms, the final state is the ferromagnetic configuration (inset on the right). The saddle points (insets on the top) correspond to the highest-energy point along the minimum energy paths and define the energy barriers.

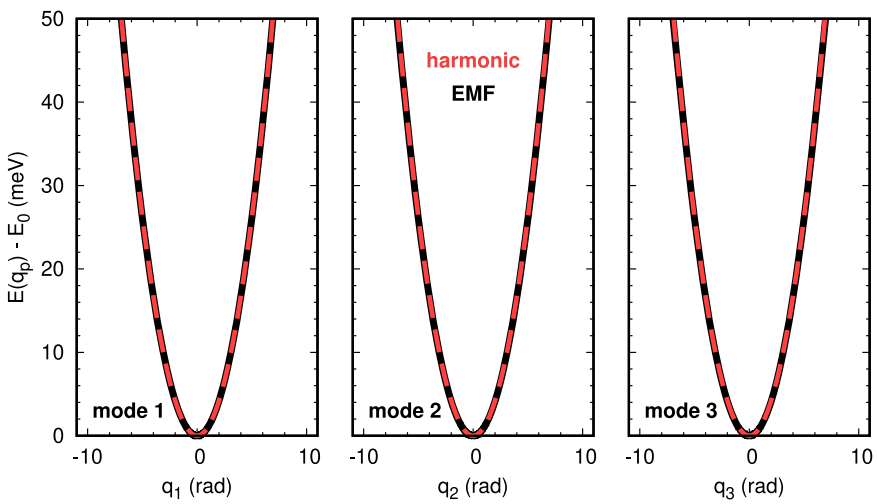


Fig. 5 | Energy curves of spin wave modes in Pd-fcc/Fe/Ir(111). An out-of-plane magnetic field of 4.0 T is assumed. The black lines show the energies relative to the ferromagnetic state and are obtained by EMF. The red dashed lines are constructed from the eigenvalues of the Hessian of the ferromagnetic state via Eq. (7).

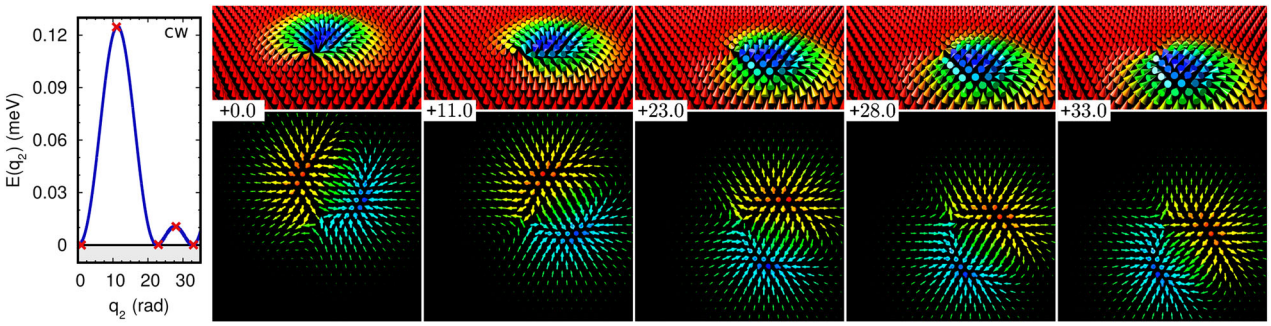


Fig. 8 | Second chimera saddle point mode analysed via EMF. The energy dispersion over the total geodesic distance, q_2, of a $2\pi/3$ clockwise rotation is shown on the left. For the positions marked with a cross, the magnetic structures and the corresponding eigenvectors are shown on the right. The colour codes decode the out-of-plane components, respectively. In the corners, the geodesic distance is shown in rad. Figure adapted from ref. 53.

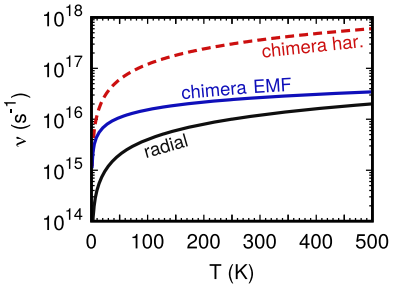


Fig. 9 | Prefactor of skyrmion collapse via radial and chimera transition mechanisms for varying temperatures. As system parameters, the Pd-fcc/Fe/Ir(111) system with 4.0 T out-of-plane has been used. The rotational eigenmode of the chimera saddle point was modelled via eigenmode following (blue) and harmonic approximation (red). Note that the prefactor of the radially symmetric collapse (black) has been multiplied by a factor of two to take into account the two saddle points per unit cell. Fig. adapted from ref. 53.

Bloch-like point changes periodically, leading to the two different peaks visible in the 120° energy curve.

Overall, the revealed energy variation along this eigenmode is quite small, which makes it negligible at non-zero temperatures and allows for the quasi-free rotation via zero-mode approximation. Combined with the obtained understanding about the nature of this eigenmode by EMF, adequate analytical modelling of this mode became feasible[39].

The direct entropy calculation of the chimera rotation mode is achieved by numerically integrating the Boltzmann factor of the energy curve over the interval of a full rotation (see Eq. (7)). The obtained partial partition function, Φ_2, is plugged into the formula of the prefactor in Eq. (3), in which the partial partition functions of the other eigenmodes are considered in harmonic approximation. The resulting prefactor is shown in Fig. 9.

The prefactor of the chimera transition mechanism obtained by EMF increases fast at very low temperatures, as the low rotation barrier initially forces the chimera state to vibrate around its energetically favourable orientation, and more states are available for occupation. With increasing temperature, this occupation starts to saturate as the rotation eigenmode changes from vibration to quasi-free rotation at higher temperatures. This causes the prefactor to change from a $\propto T$-like growth to a $\propto \sqrt{T}$ like growth, stemming from the ratio of zero-modes between the initial skyrmion state with its two translational zero-modes and the saddle point state. Each zero-mode at the initial and saddle point state adds or subtracts a factor of $\propto \sqrt{T}$ to the temperature dependency of the prefactor[21].

In contrast to the results of the eigenmode following method, the harmonic approximation of the rotational eigenmode never yields a transition from its vibrational character to a quasi-free rotation. Instead, it assumes that more and more states can be occupied even when these in reality are not available, as the system cannot occupy more rotational degrees of freedom than the completely free rotation at high temperatures. Consequently, this unphysical modelling by the harmonic approximation yields a continuous $\propto T$ like growth of the prefactor, overestimating the prefactor with increasing temperature.

For completeness, the prefactor of the radial collapse is shown, too. It exhibits the typical $\propto T$ like behaviour[21] as it does not have the rotational degree of freedom, which also means less available states to occupy and thus a lower overall prefactor compared to the chimera transition rates. Therefore, it can be interpreted that entropic effects favour the chimera transition state as it offers combinatorially more states to pass the energy barrier.

Rotation of the chimera saddle point state under an in-plane magnetic field

In Fig. 10a, the energy curve of the chimera rotation mode is displayed again, this time for more than a full clockwise and anti-clockwise rotation, respectively, which amounts to a distance of around ± 100rad. The energy exhibits the same 3-fold symmetry in the energy curve on the order of 0.1 meV as it was already discussed in the last section. By applying an in-plane magnetic field of 0.1T to the magnetic layer, the 3-fold symmetry of the rotation of the chimera state is broken, creating a preferred orientation of the in-plane components of the moments along the field. This creates a single energy barrier to the rotational movement of about 1.5 meV with some modulations due to the lattice effect. This barrier scales linearly with the magnetic field, and consequently, a field strength of 0.2 T yields twice the energy barrier of slightly over 3.0 meV.

At this field strength, the barrier became almost symmetrical. As it is much larger than the original barrier stemming solely from lattice effects and DMI, the interval in which the harmonic approximation can be expected to be accurate is shifting towards higher values as before. The structure will vibrate around the optimal orientation and be trapped in its vicinity for small temperatures. In contrast, the chimera state can almost freely rotate for large temperatures, only slightly modified by the in-plane magnetic field barrier. This way, the in-plane field opens an intermediate regime between these two extreme cases in which the situation is more complex and both analytical approximations are expected to fail. Therefore, it represents an excellent use case for the EMF method, which is able to calculate the partial partition function for a continuous temperature spectrum, which traditionally was not achievable.

Calculating the partial partition function, ϕ_p, with these three different approaches for varying temperatures yields the data of Fig. 11. Naturally, the value corresponding to the zero-mode approximation is constant since the occupation of free rotational states is independent of temperature. On the contrary, the harmonic approximation reflects an unphysical and ever-increasing occupation of states for increasing thermal energy.

The curve corresponding to EMF, however, is showing a more balanced behaviour. For very low temperatures, it does coincide with the

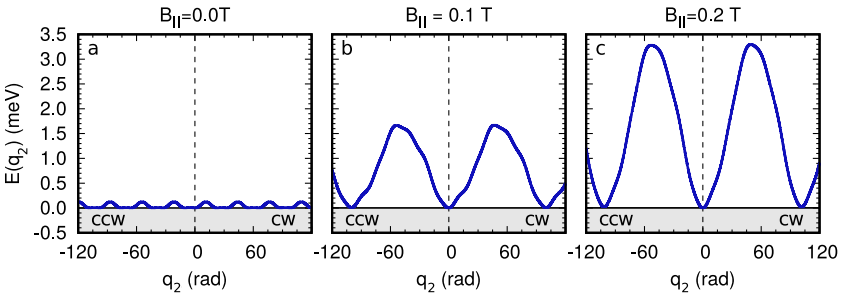


Fig. 10 | Energy of the chimera-saddle-point rotation under an in-plane magnetic field. The clockwise (cw) and anticlockwise (ccw) rotations are shown for slightly more than one full period. An in-plane field of 0.0 T (**a**), 0.1 T (**b**), and 0.2 T (**c**) is applied in the positive x-direction, which aligns with the initial orientation of the chimera skyrmion saddle point state, which is also the energy reference in each plot, respectively. The magnetic system is Pd-fcc/Fe/Ir(111) with an additional out-of-plane field of 4.0 T. Fig. adapted from ref. 53.

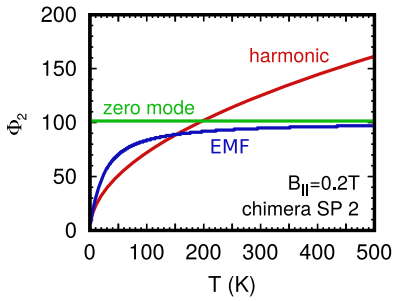


Fig. 11 | Comparison of the partial partition function, Φ_2, of the second chimera saddle point eigenmode over temperature. The values are obtained numerically via EMF (blue), harmonic (red) or zero-mode approximation (green) for a skyrmion collapse via the chimera transition mechanism in Pd-fcc/Fe/Ir(111) with an external field of $B_\perp$ = 4.0T and $B_\parallel$ = 0.2T. Figure adapted from ref. 53.

values of the harmonic approximation. It increases faster than the curve of the harmonic approximation up to values of roughly 150K, where they cross, and the EMF curve starts to slowly converge against the constant value of the zero-mode approximation.

In this way, the EMF method closes the gap between the two temperature regimes of the harmonic and the zero mode approximations while still correctly reproducing the extremal behaviour on both ends. Note that without the data of the EMF curve, there would be no information about when the zero mode and harmonic approximations over- or underestimate the occupation and hence, when they are valid or failing. The EMF methods are doing both, enabling the evaluation of the quality of the two approximations as well as calculating the partial partition functions over all temperatures, including the area in which the analytical approximations are failing.

Discussion

The EMF method for direct entropy calculation has been introduced, which combines eigenmode following with the numerical evaluation of the occupation along the way. The mathematical and physical background has been provided and formulated for a generic 3N system, allowing for the adaptation of the EMF method to various fields in physics and chemistry. Further, the technical concept and algorithm of the EMF have been explained in detail, including mode tracking, which enables the following of an arbitrarily selected eigenmode.

We demonstrated how the entropy of a system can be calculated by a case-dependent treatment of eigenmodes by harmonic approximation, zero-mode approximation and EMF, which can be adapted to the requirements of the system. These requirements do not need to be known a priori. Instead, very soft or problematic eigenmodes can be pre-determined by the eigenspectrum of the Hessian matrix and subsequently characterised by EMF, as we have demonstrated for the rotation mode of the chimera saddle point state.

Going away from the general 3*N* formulation, we used 2*N* atomistic spin simulations of magnetic systems to provide hands-on examples of EMF calculations. The single spin system with anisotropy already showed the limitations of the harmonic and zero-mode approximations, while the EMF method described all cases adequately, reproducing the reference values. The eigenmodes of the ferromagnetic state in the exchange frustrated Pd-fcc/Fe/Ir(111) system provided an estimate for the accuracy of the numerical integration of partial partition functions in a realistic 50 × 50 simulation box. Moreover, the application of EMF revealed that the energy curves of these spin wave modes can be modelled parabolically even in the presence of strong exchange frustration in Pd-fcc/Fe/Ir(111).

The investigation of the rotation eigenmode of the chimera transition state of skyrmion annihilation represents the first real use case of the EMF method. First, it revealed the character and energy curve of the eigenmode, identifying it as a rotation mode. Then, it has been successfully applied to calculate the mean transition rates of skyrmion collapse in the framework of transition state theory beyond harmonic approximation. The addition of an in-plane magnetic field raises a rotation barrier for the chimera state. It has been used to demonstrate the capability of the EMF method to calculate the partial partition function for the entire temperature regime, which has not been possible before. Other real-life use cases and their publications have been referenced.

Overall, we demonstrated that the EMF method is well-suited for treating eigenmodes with non-paraboloid-shaped energy curves, which has not been done in magnetism before. It is easy to implement as it requires at least partial diagonalization of the Hessian matrix, which will already be implemented in most pre-existing codes, as it is the basis for the harmonic approximation approach. The application is feasible and effective, even for 50 × 50 simulation boxes in the case of atomistic simulations, and especially when combined with a harmonic approximation for the most eigenmodes of a large system. This makes the EMF method well-suited for applications in a large variety of systems, and we are expecting it to play a role in the further development of "beyond harmonic" entropy and partition function calculation methods.

In its state of development, the EMF method does not solve the problem of coupled eigenmodes and is strictly speaking only applicable when the coupling of the following eigenmode to the rest of the spectrum is negligible. However, we deem a cross-sampling extension of the method for two or more eigenmodes possible, which could be the subject of further development. In its current form, the single eigenmode form, however, it already makes entropy and lifetimes calculations of systems with non-parabolic energy curves, such as chimera or antiskyrmion states, possible. While it remains to be seen if the EMF method can be transferred directly to quantum mechanical methods such as DFT, we believe that it can be useful in a wide range of fields in physics and chemistry.

Methods

Simulation details

All atomistic spin simulations have been performed with Spinaker and its predecessor, the Kiel simulation code. Both codes were developed in collaboration with the University of Kiel and the University of Iceland. The

EMF method is implemented with a simple Euler rotation step, realising a geodesic displacement along the selected eigenvector. The EMF calculations typically consist of 10,000 to 20,000 such steps with a constant width of $0.5 - 1.0{*}10^{-4}$ rad. For the spin wave eigenmodes of the ferromagnetic state shown in Fig. 6, a step width of 0.01 has been applied for 1000 Euler steps each. Magnetic textures were energetically relaxed via spin-dynamics, vpo or the lbfgs algorithm with applied periodic boundary conditions. MEPs and saddle points have been obtained via CI-GNEB.

Calculations of the partition functions of a single spin with various methods

Here we provide the details on how the values in Table 1 have been obtained. In a single spin system with uniaxial anisotropy along $\hat{\mathbf{z}}$, the energy is given by

$$E = -K\, m_z^2 \tag{10}$$

$$= -K\cos^2(\vartheta). \tag{11}$$

The strength of the anisotropy is $K = 1$ meV, and the resulting energy of the ground state is $E_0 = -1$ meV.

In the case of the spin being exactly aligned with the easy axis, there is a two-fold degenerate eigenmode describing the direct rotation from pole to pole. Its partition function is given by

$$\Phi_{\mathrm{min},1} = \int e^{-\beta[E(\vartheta)-E_0]}\, d\vartheta \tag{12}$$

$$= \int e^{-\beta K[\cos^2(\vartheta)-1]}\, d\vartheta \tag{13}$$

In harmonic approximation and with the eigenvalue of the Hessian, $\lambda_1 = 2$ meV, the integral simplifies to

$$\Phi^{\mathrm{harm}}_{\mathrm{min},1} = 2.0 * \sqrt{\frac{2\pi}{\beta\lambda_1}} \tag{14}$$

$$\approx 3.291. \tag{15}$$

The combinational factor of two stems from the two local minima at $\pm\hat{\mathbf{z}}$ which are approximated by one parabola each and both contribute to the occupied states when considering a full rotation.

In zero mode approximation, the integral reads

$$\begin{aligned}\Phi^{\mathrm{zero}}_{\mathrm{min},1} &= \textstyle\int_0^{2\pi} e^{-\beta[E(\vartheta=0)-E_0]}\, d\vartheta \\ &= \textstyle\int_0^{2\pi} 1\, d\vartheta \\ &= 2\pi\end{aligned} \tag{16}$$

For a solution without approximating the energy function, we use equation (13) and solve it by direct numerical integration over ϑ. This is possible because the trajectory of the eigenmode is trivial and known: a straight rotation from $+\hat{\mathbf{z}}$ to $-\hat{\mathbf{z}}$ and back on the other side of the sphere. Numerical integration in this context simply means to approximate the integral by a summation over finite steps in which the local value of the function is calculated. For the application of the EMF method, the initial spin orientation is very slightly rotated away from the easy axis to avoid the initial degeneracy. However, this is done for numerical reasons, and the effect on the result is highly negligible.

In the case of the spin being in SP configuration, i.e., it lies in the equatorial plane, the diagonalisation of the Hessian yields two distinct eigenmodes. The first is similar in character to the two-fold degenerated mode of the energy minimum state we just discussed. The second corresponds to a rotation around the equator. Both eigenmodes cannot be integrated in a harmonic approximation: The eigenvalue of the first eigenmode is negative (−2 meV), and the second eigenvalue is zero. To calculate them in zero mode approximation, we assume that the system has the constant energy of the saddle point state, $E_0^{\mathrm{SP}} = E(\vartheta = \pi/2) = 0.0$ meV, which is a bad approximation for the first eigenmode but an excellent one for the second.

For the first SP eigenmode in zero mode approximation, we get

$$\Phi^{\mathrm{zero}}_{\mathrm{SP},1} = \int_0^{2\pi} e^{-\beta[E(\vartheta=\pi/2)-E_0^{\mathrm{SP}}]}\, d\vartheta \tag{17}$$

$$= 2\pi\, e^{\beta E_0^{\mathrm{SP}}} \tag{18}$$

$$\approx 1.969. \tag{19}$$

The second SP eigenmode in zero mode approximation yields the same value as we just integrate the same constant over a full period over φ instead of ϑ:

$$\Phi^{\mathrm{zero}}_{\mathrm{SP},2} = \int_0^{2\pi} e^{-\beta[E(\varphi=\pi/2)-E_0^{\mathrm{SP}}]}\, d\varphi \tag{20}$$

$$= 2\pi\, e^{\beta E_0^{\mathrm{SP}}} \tag{21}$$

$$\approx 1.969\,. \tag{22}$$

Both eigenmodes can be solved numerically by applying the direct numerical integrations of ϑ and φ, respectively, whose trajectories are trivial. The EMF method can be applied without any special considerations.

Data availability

The data that support the findings of this study are available from the corresponding author upon reasonable request.

Code availability

The underlying code for this study is available upon reasonable request from the corresponding or last author.

Received: 24 January 2025; Accepted: 30 April 2026;
Published online: 13 July 2026

References

1. Schlegel, H. B. Exploring potential energy surfaces for chemical reactions: an overview of some practical methods. *J. Comput. Chem.* **24**, 1514–1527 (2003).
2. Doye, J. & Wales, D. Surveying a potential energy surface by eigenvector-following: applications to global optimisation and the structural transformations of clusters. *Z. f.ür. Phys. D. At. Mol. Clust.* **40**, 194–197 (1997).
3. Steinmetzer, J., Kupfer, S. & Gräfe, S. pysisyphus: Exploring potential energy surfaces in ground and excited states. *Int. J. Quantum Chem.* **121**, e26390 (2021).
4. Nichols, J., Taylor, H., Schmidt, P. & Simons, J. Walking on potential energy surfaces. *J. Chem. Phys.* **92**, 340–346 (1990).
5. Baker, J. An algorithm for the location of transition states. *J. Comput. Chem.* **7**, 385–395 (1986).
6. Banerjee, A., Adams, N., Simons, J. & Shepard, R. Search for stationary points on surfaces. *J. Phys. Chem.* **89**, 52–57 (1985).
7. Olsen, R., Kroes, G., Henkelman, G., Arnaldsson, A. & Jónsson, H. Comparison of methods for finding saddle points without knowledge of the final states. *J. Chem. Phys.* **121**, 9776–9792 (2004).

8. Cerjan, C. J. & Miller, W. H. On finding transition states. *J. Chem. Phys.* **75**, 2800–2806 (1981).
9. Henkelman, G. & Jónsson, H. A dimer method for finding saddle points on high dimensional potential surfaces using only first derivatives. *J. Chem. Phys.* **111**, 7010–7022 (1999).
10. Müller, G. P. et al. Duplication, collapse, and escape of magnetic skyrmions revealed using a systematic saddle point search method. *Phys. Rev. Lett.* **121**, 197202 (2018).
11. Jónsson, H., Mills, G. & Jacobsen, K. W. *Nudged Elastic Band Method for Finding Minimum Energy Paths of Transitions* (World Scientific, 1998).
12. Sheppard, D., Xiao, P., Chemelewski, W., Johnson, D. D. & Henkelman, G. A generalized solid-state nudged elastic band method. *J. Chem. Phys*. **136**, 074103 (2012).
13. Henkelman, G. & Jónsson, H. Improved tangent estimate in the nudged elastic band method for finding minimum energy paths and saddle points. *J. Chem. Phys.* **113**, 9978–9985 (2000).
14. Wigner, E. The transition state method. *Trans. Faraday Soc.* **34**, 29–41 (1938).
15. Evans, M. G. & Polanyi, M. Some applications of the transition state method to the calculation of reaction velocities, especially in solution. *Trans. Faraday Soc.* **31**, 875–894 (1935).
16. Eyring, H. & Polanyi, M. Über einfache Gasreaktionen. *Z. f.ür. Phys. Chem. Abt. B* **12**, 279–311 (1931).
17. Glasstone, S., Laidler, K. J. & Eyring, H. *The Theory of Rate Processes: the Kinetics of Chemical Reactions, Viscosity, Diffusion and Electrochemical Phenomena,* (McGraw-Hill, 1941).
18. Langer, J. S. Statistical theory of the decay of metastable states. *Ann. Phys.* **54**, 258–275 (1969).
19. Henkelman, G., Uberuaga, B. P. & Jónsson, H. A climbing image nudged elastic band method for finding saddle points and minimum energy paths. *J. Chem. Phys.* **113**, 9901–9904 (2000).
20. Beste, A. One-dimensional anharmonic oscillator: Quantum versus classical vibrational partition functions. *Chem. Phys. Lett.* **493**, 200–205 (2010).
21. von Malottki, S., Bessarab, P. F., Haldar, S., Delin, A. & Heinze, S. Skyrmion lifetime in ultrathin films. *Phys. Rev. B* **99**, 060409 (2019).
22. Desplat, L., Suess, D., Kim, J.-V. & Stamps, R. L. Thermal stability of metastable magnetic skyrmions: Entropic narrowing and significance of internal eigenmodes. *Phys. Rev. B* **98**, 134407 (2018).
23. Dittrich, R. et al. A path method for finding energy barriers and minimum energy paths in complex micromagnetic systems. *J. Magn. Magn. Mater.* **250**, 12–19 (2002).
24. Thiaville, A., García, J. M., Miltat, J., Schrefl, T. et al. Micromagnetic study of bloch-point-mediated vortex core reversal. *Phys. Rev. B* **67**, 094410 (2003).
25. Krone, P., Makarov, D., Albrecht, M., Schrefl, T. & Suess, D. Magnetization reversal processes of single nanomagnets and their energy barrier. *J. Magn. Magn. Mater.* **322**, 3771–3776 (2010).
26. Dittrich, R. et al. Energy barriers in magnetic random access memory elements. *IEEE Trans. Magn.* **39**, 2839–2841 (2003).
27. Muehlbauer, S. et al. Skyrmion lattice in a chiral magnet. *Science* **323**, 915–919 (2009).
28. Back, C. et al. The 2020 skyrmionics roadmap. *J. Phys. D Appl. Phys.* **53**, 363001 (2020).
29. Tokura, Y. & Kanazawa, N. Magnetic skyrmion materials. *Chem. Rev.* **121**, 2857–2897 (2020).
30. Göbel, B., Mertig, I. & Tretiakov, O. A. Beyond skyrmions: Review and perspectives of alternative magnetic quasiparticles. *Phys. Rep.* **895**, 1–28 (2021).
31. Heinze, S. et al. Spontaneous atomic-scale magnetic skyrmion lattice in two dimensions. *Nat. Phys.* **7**, 713–718 (2011).
32. Bessarab, P. F., Uzdin, V. M. & Jónsson, H. Method for finding mechanism and activation energy of magnetic transitions, applied to skyrmion and antivortex annihilation. *Comput. Phys. Commun.* **196**, 335–347 (2015).
33. Lobanov, I. S., Jónsson, H. & Uzdin, V. M. Mechanism and activation energy of magnetic skyrmion annihilation obtained from minimum energy path calculations. *Phys. Rev. B* **94**, 174418 (2016).
34. von Malottki, S., Dupé, B., Bessarab, P. F., Delin, A. & Heinze, S. Enhanced skyrmion stability due to exchange frustration. *Sci. Rep.* **7**, 12299 (2017).
35. Desplat, L., Kim, J.-V. & Stamps, R. L. Paths to annihilation of first-and second-order (anti) skyrmions via (anti) meron nucleation on the frustrated square lattice. *Phys. Rev. B* **99**, 174409 (2019).
36. Meyer, S. et al. Isolated zero field sub-10 nm skyrmions in ultrathin co films. *Nat. Commun.* **10**, 3823 (2019).
37. Bessarab, P. F. et al. Lifetime of racetrack skyrmions. *Sci. Rep.* **8**, 3433 (2018).
38. Muckel, F. et al. Experimental identification of two distinct skyrmion collapse mechanisms. *Nat. Phys.* **17**, 395–402 (2021).
39. Goerzen, M. A., von Malottki, S., Meyer, S., Bessarab, P. F. & Heinze, S. Lifetime of coexisting sub-10 nm zero-field skyrmions and antiskyrmions. *npj Quant. Mater.* **8**, 54 (2023).
40. Hoffmann, M., Müller, G. P., Melcher, C. & Blügel, S. Skyrmion-antiskyrmion racetrack memory in rank-one dmi materials. *Front. Phys.* **9**, 769873 (2021).
41. Bessarab, P. F. et al. Stability and lifetime of antiferromagnetic skyrmions. *Phys. Rev. B* **99**, 140411 (2019).
42. Paul, S., Haldar, S., von Malottki, S. & Heinze, S. Role of higher-order exchange interactions for skyrmion stability. *Nat. Commun.* **11**, 4756 (2020).
43. Schrautzer, H., von Malottki, S., Bessarab, P. F. & Heinze, S. Effects of interlayer exchange on collapse mechanisms and stability of magnetic skyrmions. *Phys. Rev. B* **105**, 014414 (2022).
44. Hoffmann, M., Müller, G. P. & Blügel, S. Atomistic perspective of long lifetimes of small skyrmions at room temperature. *Phys. Rev. Lett.* **124**, 247201 (2020).
45. Hagemeister, J., Siemens, A., Rózsa, L., Vedmedenko, E. Y. & Wiesendanger, R. Controlled creation and stability of kπ skyrmions on a discrete lattice. *Phys. Rev. B* **97**, 174436 (2018).
46. Leishman, A. et al. Topological energy barrier for skyrmion lattice formation in mnsi. *Phys. Rev. B* **102**, 104416 (2020).
47. Birch, M. T. et al. Topological defect-mediated skyrmion annihilation in three dimensions. *Commun. Phys.* **4**, 175 (2021).
48. Bessarab, P. F., Uzdin, V. M. & Jónsson, H. Harmonic transition-state theory of thermal spin transitions. *Phys. Rev. B* **85**, 184409 (2012).
49. Varentcova, A. S. et al. Toward room-temperature nanoscale skyrmions in ultrathin films. *npj Comput. Mater.* **6**, 1–11 (2020).
50. Goerzen, M. A., von Malottki, S., Kwiatkowski, G. J., Bessarab, P. F. & Heinze, S. Atomistic spin simulations of electric-field-assisted nucleation and annihilation of magnetic skyrmions in Pd/Fe/Ir (111). *Phys. Rev. B* **105**, 214435 (2022).
51. Haldar, S., von Malottki, S., Meyer, S., Bessarab, P. F. & Heinze, S. First-principles prediction of sub-10-nm skyrmions in Pd/Fe bilayers on Rh (111). *Phys. Rev. B* **98**, 060413 (2018).
52. Wild, J. et al. Entropy-limited topological protection of skyrmions. *Sci. Adv.* **3**, e1701704 (2017).
53. von Malottki, S. *Stability of Magnetic Skyrmions in Ultrathin Films*. Ph.D. thesis, Christian-Albrechts-Universität zu Kiel (2021).
54. Rohart, S., Miltat, J. & Thiaville, A. Path to collapse for an isolated néel skyrmion. *Phys. Rev. B* **93**, 214412 (2016).
55. Hagemeister, J., Romming, N., Von Bergmann, K., Vedmedenko, E. & Wiesendanger, R. Stability of single skyrmionic bits. *Nat. Commun.* **6**, 8455 (2015).
56. Desplat, L., Vogler, C., Kim, J.-V., Stamps, R. L. & Suess, D. Path sampling for lifetimes of metastable magnetic skyrmions and direct comparison with Kramers' method. *Phys. Rev. B* **101**, 060403 (2020).

57. Collinge, G. et al. Effect of collective dynamics and anharmonicity on entropy in heterogenous catalysis: Building the case for advanced molecular simulations. *ACS Catal.* **10**, 9236–9260 (2020).
58. Jørgensen, M. & Gronbeck, H. Adsorbate entropies with complete potential energy sampling in microkinetic modeling. *J. Phys. Chem. C.* **121**, 7199–7207 (2017).
59. Amsler, J., Plessow, P. N., Studt, F. & Bucko, T. Anharmonic correction to adsorption free energy from DFT-based MD using thermodynamic integration. *J. Chem. Theory Comput.* **17**, 1155–1169 (2021).
60. Sauer, J. The future of computational catalysis. *J. Catal.* **433**, 115482 (2024).
61. Monacelli, L. et al. The stochastic self-consistent harmonic approximation: calculating vibrational properties of materials with full quantum and anharmonic effects. *J. Phys. Condens. Matter* **33**, 363001 (2021).
62. Li, H., Paolucci, C. & Schneider, W. F. Zeolite adsorption free energies from ab initio potentials of mean force. *J. Chem. Theory Comput.* **14**, 929–938 (2018).
63. Sprowl, L. H., Campbell, C. T. & Arnadottir, L. Hindered translator and hindered rotor models for adsorbates: Partition functions and entropies. *J. Phys. Chem. C.* **120**, 9719–9731 (2016).
64. Piccini, G. & Sauer, J. Quantum chemical free energies: Structure optimization and vibrational frequencies in normal modes. *J. Chem. Theory Comput.* **9**, 5038–5045 (2013).
65. Piccini, G. & Sauer, J. Effect of anharmonicity on adsorption thermodynamics. *J. Chem. Theory Comput.* **10**, 2479–2487 (2014).
66. Plasencia Gutiérrez, M., Argaez, C. & Jonsson, H. Improved minimum mode following method for finding first order saddle points. *J. Chem. Theory Comput.* **13**, 125–134 (2017).
67. Tsai, C. & Jordan, K. Use of an eigenmode method to locate the stationary points on the potential energy surfaces of selected argon and water clusters. *J. Phys. Chem.* **97**, 11227–11237 (1993).
68. Romming, N. et al. Writing and deleting single magnetic skyrmions. *Science* **341**, 636–639 (2013).
69. Vlasov, S. M. et al. Magnetic skyrmion annihilation by quantum mechanical tunneling. *N. J. Phys.* **22**, 083013 (2020).
70. Kollwitz, L., Goerzen, M. A., Beyer, B., Schrautzer, H. & Heinze, S. Entropy-driven phase transition in a non-collinear antiferromagnet due to higher-order exchange interactions. *npj Spintron.* **4**, 2 (2026).
71. Stewart, G. W. A Krylov–Schur algorithm for large eigenproblems. *SIAM J. Matrix Anal. Appl.* **23**, 601–614 (2002).
72. Sallermann, M., Jónsson, H. & Blügel, S. Stability of hopfions in bulk magnets with competing exchange interactions. *Phys. Rev. B* **107**, 104404 (2023).
73. Schrautzer, H., Sallermann, M., Bessarab, P. F. & Jónsson, H. Identification of mechanisms of magnetic transitions using an efficient method for converging on first-order saddle points. *Phys. Rev. B* **112**, 104433 (2025).
74. Dupé, B., Hoffmann, M., Paillard, C. & Heinze, S. Tailoring magnetic skyrmions in ultra-thin transition metal films. *Nat. Commun.* **5**, 4030 (2014).
75. Böttcher, M., Heinze, S., Egorov, S., Sinova, J. & Dupé, B. B–t phase diagram of pd/fe/ir (111) computed with parallel tempering Monte Carlo. *N. J. Phys.* **20**, 103014 (2018).
76. Desplat, L. & Dupé, B. Eigenmodes of magnetic skyrmion lattices. *Phys. Rev. B* **107**, 144415 (2023).
77. Romming, N., Kubetzka, A., Hanneken, C., von Bergmann, K. & Wiesendanger, R. Field-dependent size and shape of single magnetic skyrmions. *Phys. Rev. Lett.* **114**, 177203 (2015).
78. Hsu, P.-J. et al. Electric-field-driven switching of individual magnetic skyrmions. *Nat. Nanotechnol.* **12**, 123–126 (2017).
79. Lindner, P. et al. Temperature and magnetic field dependent behavior of atomic-scale skyrmions in Pd/Fe/Ir(111) nanoislands. *Phys. Rev. B* **101**, 214445 (2020).

Acknowledgements

S.v.M. gratefully acknowledges funding of the Deutsche Forschungsgemeinschaft (DFG) via a Walter Benjamin-Stipendium with project number 523127890 as well as funding from the Fonds National de la Recherche Scientifique (FNRS) under project number 1.B.504.24. H.S. gratefully acknowledges financial support from the Icelandic Research Fund (Grant No. 239435). P.F.B. gratefully acknowledges financial support from the Icelandic Research Fund (Grants No. 217750 and 2410333), the University of Iceland Research Fund (Grant No. 15673), the Swedish Research Council (Grant No. 2020-05110), and the Crafoord Foundation (Grant No. 20231063). M.A.G. and S.H. gratefully acknowledge financial support from the DFG through SPP2137 “Skyrmionics” (Project No. 462602351). We thank Dr. Johannes Steinmetzer and Prof. Henrik Grönbeck for helpful discussions.

Author contributions

S.v.M., M.A.G., and H.S. performed the calculations. S.v.M. conceived the project and developed the EMF method and its original implementation in the Kiel simulation code. M.A.G. optimised the implementation. H.S. implemented the EMF method in the Spinaker code and further optimised it. All authors contributed to the analysis and discussion of the simulation results. S.v.M., M.A.G., and H.S. wrote the first version of the manuscript, and all authors contributed to the final version.

Funding

Open Access funding enabled and organized by Projekt DEAL.

Competing interests

The authors declare no competing interests.

Additional information

Supplementary information The online version contains supplementary material available at https://doi.org/10.1038/s41524-026-02130-w.

Correspondence and requests for materials should be addressed to Stephan von Malottki or Stefan Heinze.

Reprints and permissions information is available at http://www.nature.com/reprints

Publisher’s note Springer Nature remains neutral with regard to jurisdictional claims in published maps and institutional affiliations.

Open Access This article is licensed under a Creative Commons Attribution 4.0 International License, which permits use, sharing, adaptation, distribution and reproduction in any medium or format, as long as you give appropriate credit to the original author(s) and the source, provide a link to the Creative Commons licence, and indicate if changes were made. The images or other third party material in this article are included in the article’s Creative Commons licence, unless indicated otherwise in a credit line to the material. If material is not included in the article’s Creative Commons licence and your intended use is not permitted by statutory regulation or exceeds the permitted use, you will need to obtain permission directly from the copyright holder. To view a copy of this licence, visit http://creativecommons.org/licenses/by/4.0/.

© The Author(s) 2026